DOI:
10.1016/j.ica.2018.11.002

Document Version
Peer reviewed version

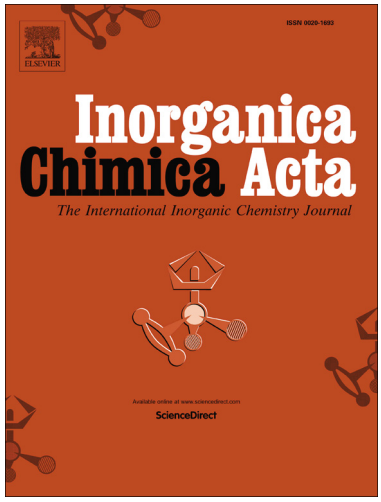

Research paper

Highly efficient electrocatalytic proton-reduction by coordinatively and electronically unsaturated Fe(CO)(κ ^{2}-dppn)(κ ^{2}-tdt)

Shishir Ghosh, Shahed Rana, Shariff E. Kabir, Michael G. Richmond, Graeme Hogarth

PII: S0020-1693(18)31358-6
DOI: https://doi.org/10.1016/j.ica.2018.11.002
Reference: ICA 18617

To appear in: *Inorganica Chimica Acta*

Received Date: 30 August 2018
Revised Date: 2 November 2018
Accepted Date: 4 November 2018

Please cite this article as: S. Ghosh, S. Rana, S.E. Kabir, M.G. Richmond, G. Hogarth, Highly efficient electrocatalytic proton-reduction by coordinatively and electronically unsaturated Fe(CO)(κ ^{2}-dppn)(κ ^{2}-tdt), *Inorganica Chimica Acta* (2018), doi: https://doi.org/10.1016/j.ica.2018.11.002

Highly efficient electrocatalytic proton-reduction by coordinatively and electronically unsaturated Fe(CO)(κ^2-dppn)(κ^2-tdt)

Shishir Ghosh[a,b,c*], Shahed Rana[b], Shariff E. Kabir[b], Michael G. Richmond[d], Graeme Hogarth[a*]

[a] *Department of Chemistry, King's College London, Britannia House, 7 Trinity Street, London SE1 1DB, UK*

[b] *Department of Chemistry, Jahangirnagar University, Savar, Dhaka-1342, Bangladesh*

[c] *Department of Chemistry, University College London, 20 Gordon Street, London WC1H OAJ, UK*

[d] *Department of Chemistry, University of North Texas, 1155 Union Circle, Box 305070, Denton, TX 76203, USA*

E-mail: sghosh_006@yahoo.com, graeme.hogarth@kcl.ac.uk

Abstract

Coordinatively and electronically unsaturated square-pyramidal Fe(CO)(κ^2-dppn)(κ^2-tdt) (**2**) is shown to be amongst the most efficient proton-reduction catalysts reported to date. It is formed from the reaction of $Fe_2(CO)_6$(μ-tdt) (tdt = 3,4-toluenedithiolate) with 1,8-bis(diphenylphosphino)naphthalene (dppn) in presence of $Me_3NO{\cdot}2H_2O$ affording $Fe_2(CO)_4$(κ^2-dppn)(μ-tdt) (**1**) as the major product, together with smaller but reproducible amounts of **2**. Both have been characterized by single crystal X-ray diffraction. The electrochemistry of **2** is solvent dependent but in both CH_2Cl_2 and in a 1:1 mixture of CH_2Cl_2/MeCN it shows a reversible reduction at $E_{1/2}$ = –1.54 V and $E_{1/2}$ = –1.68 V respectively. While **2** degrades in the presence of the strong acid $HBF_4{\cdot}2H_2O$ it is catalytically active for proton-reduction using CF_3CO_2H. Catalysis occurs at the first reduction potential and it displays an impressive i_{cat}/i_p ratio of 33 after addition of 20 equivalents CF_3CO_2H. It is amongst the most efficient molecular proton-reduction catalysts reported to date.

Keywords: Square-pyramidal; proton reduction; diphosphine; redox-active ligand; DFT

1. Introduction

The development of mononuclear iron complexes as electrocatalysts for proton-reduction is spurred on by the findings that mononuclear cobalt and nickel complexes can act as efficient catalysts for this transformation as can dithiolate-bridged diiron biomimetics of the [FeFe]-hydrogenases [1-10]. While formally electronically saturated diiron biomimics can bind a proton across the iron-iron bond, coordinatively saturated mononuclear species don't contain a free coordination site and hence a typical feature of such catalysts is reduction-induced ligand loss. Thus coordinatively unsaturated mononuclear complexes are particularly attractive targets and recently square-pyramidal iron complexes have been shown to be catalytically active by both Ott [6,7] and Jones [8] (Chart). Such systems are attractive as they operate at relatively mild reduction potentials, appear to be more robust than related diiron complexes with respect to degradation during catalysis, and hydrogen formation can be achieved using a wide range of acids.

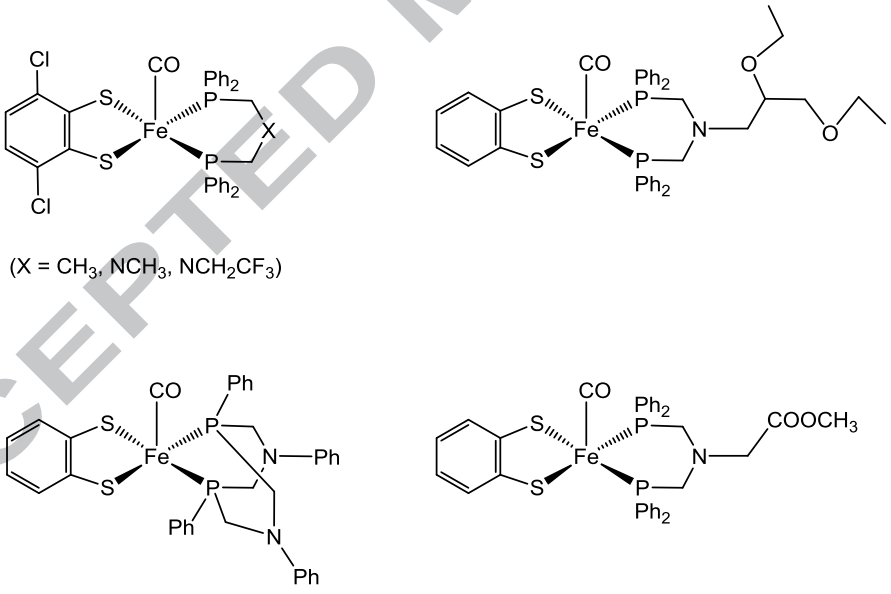

Chart Square-pyramidal iron complexes previously used as electrocatalysts for proton-reduction [6-8].

The diphosphine, 1,8-bis(diphenylphosphino)naphthalene (dppn), has attracted considerable interest as a chelating ligand due to its rigid naphthalene backbone [14-26]. During our investigations on dithiolate-bridged diiron chelate complexes, we found from the reaction of

$Fe_2(CO)_6$(μ-tdt) and dppn, in addition to the expected diiron product $Fe_2(CO)_4(\kappa^2$-dppn)(μ-tdt) (**1**), small amounts of Fe(CO)(κ^2-dppn)(κ^2-tdt) (**2**) were also formed. The highly delocalized nature of bonding in this complex, involving both chelating ligands, makes it significantly different from those studied previously [6-8] prompting us to investigate its electrocatalytic properties, the results of which are detailed herein.

2. Results and discussion

2.1. Synthesis and structure

The $Me_3NO{\cdot}2H_2O$ initiated reaction between $Fe_2(CO)_6$(μ-tdt) [27] and dppn in boiling MeCN afforded binuclear $Fe_2(CO)_4(\kappa^2$-dppn)(μ-tdt) (**1**) (35%) together with smaller amounts of 16-electron mononuclear Fe(CO)(κ^2-dppn)(κ^2-tdt) (**2**) (12%) (Scheme 1). Characterisation of both was made primarily on the basis of their crystal structure as shown in Figs. 1 and 2. Complex **1** contains a diiron framework linked by a tdt-bridge. The diphosphine chelates one iron centre, Fe(1), occupying apical-basal coordination sites with a bite angle of 87.41(3)º [Fe(1)–P(1) 2.1913(8) and Fe(1)–P(2) 2.1948(8) Å]. The Fe–Fe vector [2.5282(5) Å] is slightly elongated as compared to that in $Fe_2(CO)_6$(μ-tdt) [2.4754(14) Å] [27] and consequently Fe–S bond distances [av. 2.278(8) Å] are also slightly longer than those in $Fe_2(CO)_6$(μ-tdt) [av. 2.267(2) Å] [27]. The IR spectrum of **1** shows absorption bands at 2021s, 1950m and 1907w cm^{-1}, characteristic of $Fe_2(CO)_4(\kappa^2$-diphosphine)(μ-dithiolate) complexes, and the $^{31}P\{^1H\}$ NMR spectrum shows a singlet at δ 69.5 due to rapid apical-basal site interconversion at room temperature.

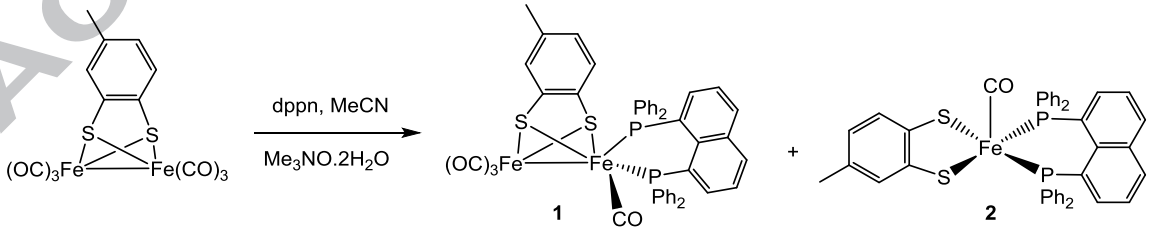

Scheme 1 Synthesis of $Fe_2(CO)_4(\kappa^2$-dppn)(μ-tdt) (**1**) and Fe(CO)(κ^2-dppn)(κ^2-tdt) (**2**).

Complex **2** co-crystallises with a molecule of chloroform and there are two short interactions between the hydrogen of this and a sulfur (2.669 Å) and carbon (2.857 Å) of the dithiolate

ligand. Complex **2** favours square-pyramidal geometry over trigonal-bipyramidal arrangement in the solid-state with the carbonyl ligand in apical position. The diphosphine and dithiolate ligands constitute the base of the pyramid and lie mutually *trans*. Metric parameters are very similar to those of related square-pyramidal complexes reported by Ott [6,7] and Jones [8].

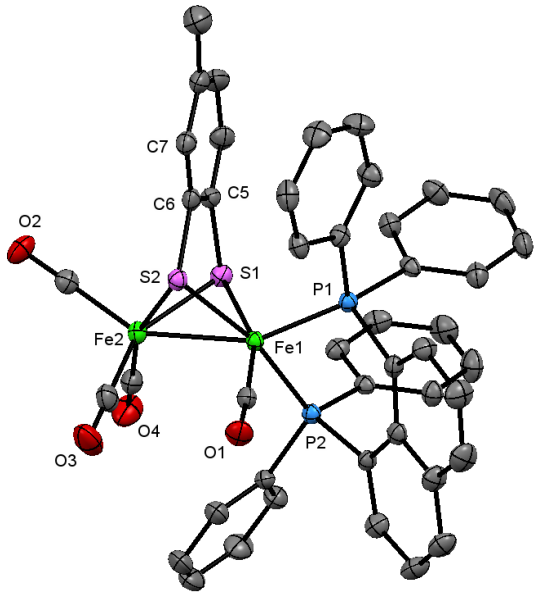

Fig. 1. ORTEP diagram of **1** (hydrogen atoms are omitted for clarity). Selected bond distances (Å) and angles (°): Fe(1)–Fe(2) 2.5282(5), Fe(1)–P(1) 2.1913(8), Fe(1)–P(2) 2.1948(8), Fe(1)–S(1) 2.2891(7), Fe(1)–S(2) 2.2680(7), Fe(2)–S(1) 2.2704(8), Fe(2)–S(2) 2.2825(8), P(1)–Fe(1)–P(2) 87.41(3), P(1)–Fe(1)–Fe(2) 154.88(3), P(2)–Fe(1)–Fe(2) 112.55(2), P(1)–Fe(1)–C(1) 94.25(9), P(2)–Fe(1)–C(1) 89.14(9), P(1)–Fe(1)–S(1) 107.64(3), P(1)–Fe(1)–S(2) 104.82(3), S(1)–Fe(1)–S(2) 79.94(3), S(1)–Fe(2)–S(2) 80.04(3), S(1)–Fe(1)–Fe(2) 55.97(2), S(1)–Fe(2)–Fe(1) 56.68(2).

Theoretical studies [7] show that simple monodentate phosphines favour hexa-coordinate complexes in reaction with dithiolate-bridged diiron complexes as the loss of CO from these octahedral complexes is energetically unfavourable, whereas the use of strongly chelating diphosphines leads to selective formation of penta-coordinate square-pyramidal complexes. Spectroscopic data for **2** are in accord with the solid-state structure. The IR spectrum shows single carbonyl absorption at 1918 cm^{-1}, being similar to those observed for related complexes [6-8]. On the basis of the solid-state structure, the two phosphorus atoms of the dppn ligand would be expected to be inequivalent, but the $^{31}P\{^{1}H\}$ NMR spectrum shows only a singlet at 67.9 ppm (at room temperature). This suggests that **2** is fluxional in solution

interchanging between square-pyramidal (**2**$_{sp}$) and trigonal-bipyramidal (**2**$_{tbp}$) geometries *via* a Berry pseudo-rotation. In support of this, Jones found that while Fe(CO){κ^2-$(Ph_2PCH_2)_2NCH_2C)_2Me$}(κ^2-bdt) (Chart) was square-planar in the solid state, the bis(diphenylphosphino)ferrocene (dppf) derivative (not shown) adopts a trigonal-bipyramidal geometry, with DFT studies revealing a small (*ca.* 6.6 kcalmol^{-1}) energy difference between conformers [7].

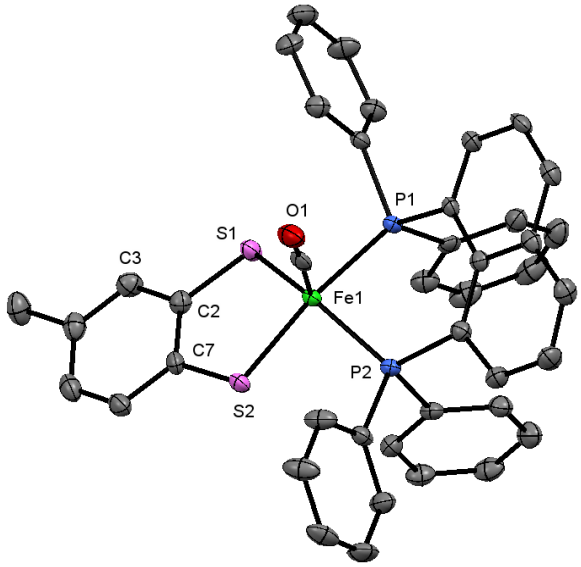

Fig. 2. ORTEP diagram of **2** (hydrogen atoms are omitted for clarity). Selected bond distances (Å) and angles (º): Fe(1)–P(1) 2.2049(7), Fe(1)–P(2) 2.1939(8), Fe(1)–S(1) 2.1889(8), Fe(1)–S(2) 2.2029(7), Fe(1)–C(1) 1.722(3), P(1)–Fe(1)–P(2) 87.97(3), S(1)–Fe(1)–S(2) 88.98(3), P(1)–Fe(1)–S(1) 88.10(3), P(2)–Fe(1)–S(2) 88.62(3), P(1)–Fe(1)–S(2) 166.59(3), P(2)–Fe(1)–S(1) 152.59(3), C(1)–Fe(1)–P(1) 90.51(9), C(1)–Fe(1)–P(2) 93.58(10), C(1)–Fe(1)–S(1) 113.57(10), C(1)–Fe(1)–S(2) 102.64(9).

2.2. Electrochemistry and DFT calculations

The redox chemistry of **2** was studied by cyclic voltammetry in both CH_2Cl_2 and a 1:1 mixture of CH_2Cl_2/MeCN (the complex is sparingly soluble in MeCN). The CV of **2** in CH_2Cl_2 at 0.1 V/s shows a reversible reduction at $E_{1/2}$ = –1.54 V (i_{an}/i_{ca} ~ 1) and an irreversible oxidation at E_p = 0.57 V (Fig. 3) and a reductive feature was observed at E_p = –0.23 V on the return scan associated with the irreversible oxidation process (Fig. S1).

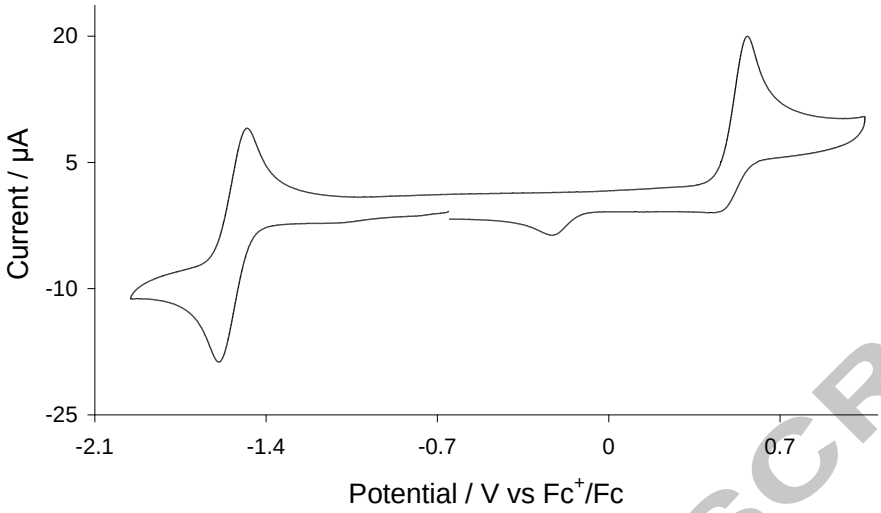

Fig. 3. CV of **2** in CH_2Cl_2 (1 mM solution, supporting electrolyte $[NBu_4][PF_6]$, scan rate 0.1 Vs^{-1}, glassy carbon electrode, potential vs Fc^+/Fc).

The oxidative wave shows some reversibility at higher scans rates (≥ 0.5 V/s), linear i_p vs $\sqrt{v}$ plots indicating that both the reductive and oxidative processes are diffusion controlled (Figs. S2 and S3). The current function ($i_p/\sqrt{v}$) associated with reduction deviates from linearity at slow scan rates (< 0.05 V/s), indicating that more than one electron may be involved in reduction at longer time scales (Fig. S4); otherwise reduction is a one-electron electrode process (in CH_2Cl_2). In a 1:1 mixture of CH_2Cl_2/MeCN (Fig. 4) some further redox features are observed, the first reversible reduction now appearing at $E_{1/2}$ = –1.68 V (i_{an}/i_{ca} ~ 0.7). A second irreversible reduction wave was also now observed at E_p = –2.21 V together with two oxidative waves, a reversible oxidation at $E_{1/2}$ = 0.22 V (i_{ca}/i_{an} ~ 0.8) followed by an irreversible wave at E_p = 0.52 V. A small reductive feature on the return scan at E_p = –0.47 V being associated with the second (irreversible) oxidative wave (Fig. S5). The enhanced reversibility of the oxidation in MeCN is probably due to metal coordination generating $[Fe(CO)(NCMe)(\kappa^2\text{-dppn})(\kappa^2\text{-tdt})]^+$, which may be sufficiently basic to stabilise against CO loss; the second irreversible oxidation wave resulting from oxidation of this solvated species. No additional features were observed when the scan rate was varied between 0.025 to 0.5 V/s (Fig. S6) and the peak current of the reversible processes exhibit a linear relationship with the square root of scan rate suggesting that both processes are diffusion controlled (Fig. S7). The current function ($i_p/\sqrt{v}$) associated with the first reductive process shows only slight deviation from linearity at very slow scan rates (< 0.05 V/s), indicating that the first reduction in CH_2Cl_2/MeCN is a one-electron electrode process (Fig. S4).

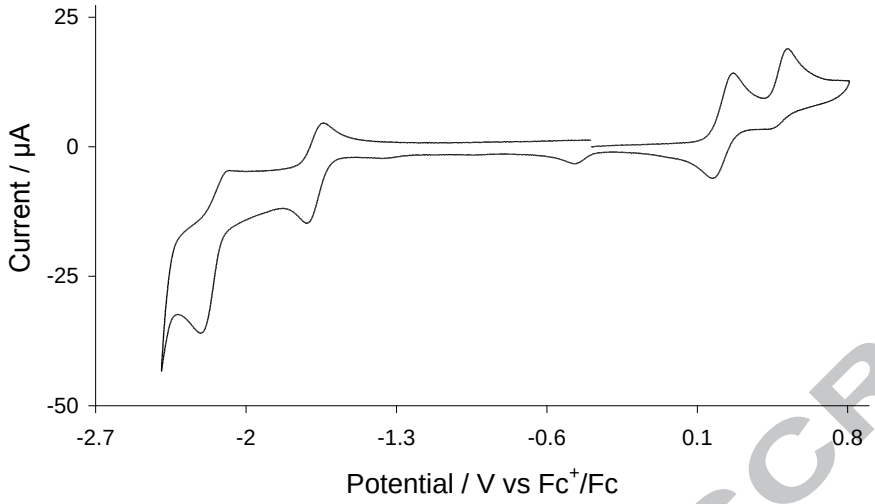

Fig. 4. CV of **2** in a 1:1 mixture of CH_2Cl_2/MeCN (1 mM solution, supporting electrolyte $[NBu_4][PF_6]$, scan rate 0.1 Vs^{-1}, glassy carbon electrode, potential vs Fc^+/Fc).

To gain insight into the redox processes we have calculated the ground state electronic structure of **2** and also the radical anion $\mathbf{2}^-$ using DFT calculations. The HOMO of **2** is delocalized over iron, one sulfur and the tolyl ring, whereas the LUMO is primarily localized on the naphthalene backbone of dppn with only a small contribution from iron (Fig. 5). Reduction of **2** results in structural modification from favoured square-pyramidal structure to a trigonal bipyramidal conformation in $\mathbf{2}^-$. The HOMO of $\mathbf{2}^-$ is similar to that in **2**, whereas the SOMO is again primarily localized on the naphthalene backbone of dppn ligand (Fig. 5). The HOMO-LUMO gap in CH_2Cl_2/MeCN (1.90 V) is *ca.* 0.2 V smaller than in CH_2Cl_2 (2.11 V), which is expected due to the coordinating nature of MeCN, which also stabilizes ionic species.

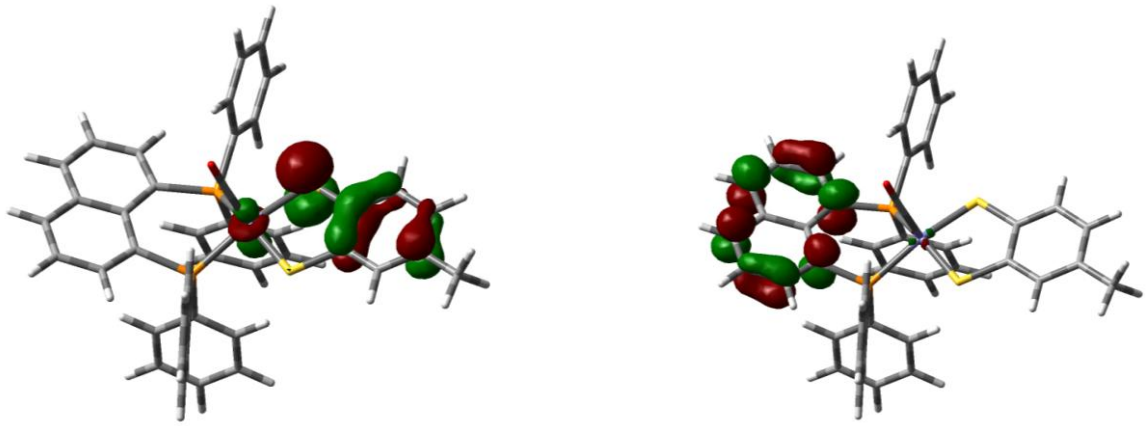

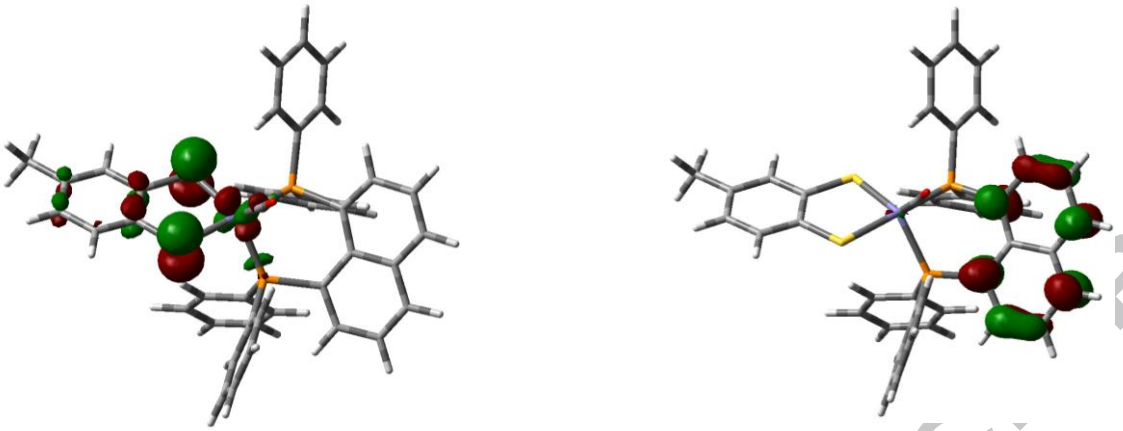

Fig. 5. HOMO (left) and LUMO (right) of **2** (top) and HOMO (left) and SOMO (right) $\mathbf{2}^-$ (bottom) (orbitals are printed with an isovalue of 0.55).

2.3. Proton-reduction catalysis

Mononuclear **2** is not protonated by a range of acids and the DFT calculations suggest that reduction is primarily ligand based, and hence it might not be expected to be an efficient proton reduction catalyst. Nevertheless, the proton reduction by **2** was tested in a 1:1 mixture of CH_2Cl_2/MeCN using CF_3CO_2H and somewhat surprisingly was found to be an efficient catalyst at around the first reduction potential (Figs. 6 and S8). Upon addition of CF_3CO_2H, two new reduction peaks were observed at E_p = –1.60 and –1.70 V (Fig. 6a) the first of which we assume corresponds to the reduction of **2** to $\mathbf{2}^-$ (as the reduction potential often displays a slight positive shift in presence of acid). At lower acid concentrations, the peak height of the first reduction was smaller than that of the second, but the peak height of the former increases as the concentration of acid is increased and surpasses the later with 10 equivalents of CF_3CO_2H, both peaks merging at higher acid concentrations (Fig. 6b). Similar behaviour was noted by Jones for related Fe(CO)(κ^2-diphosphine)(κ^2-bdt) complexes at low *p*-TsOH concentrations [7]. Since **2** does not protonate by CF_3CO_2H, then an EC mechanism is expected; reduction at E_p = –1.60 V generating $\mathbf{2}^-$ being likely followed by rapid protonation to give HFe(CO)(κ^2-dppn)(κ^2-tdt) (**2H**). Thus, although DFT calculations suggest that the reduction of **2** is dppn-centred, the HOMO of the radical anion is partially based on iron which is necessary for metal protonation. An explanation for the two closely space catalytic events could be that different isomers of **2H** are accessible resulting from proton trapping of the anion before and after Berry pseudo-rotation. Processes occurring after the initial

protonation are not accessible to us and in the absence of detailed DFT calculations we prefer not to speculate on later parts of the catalytic cycle.

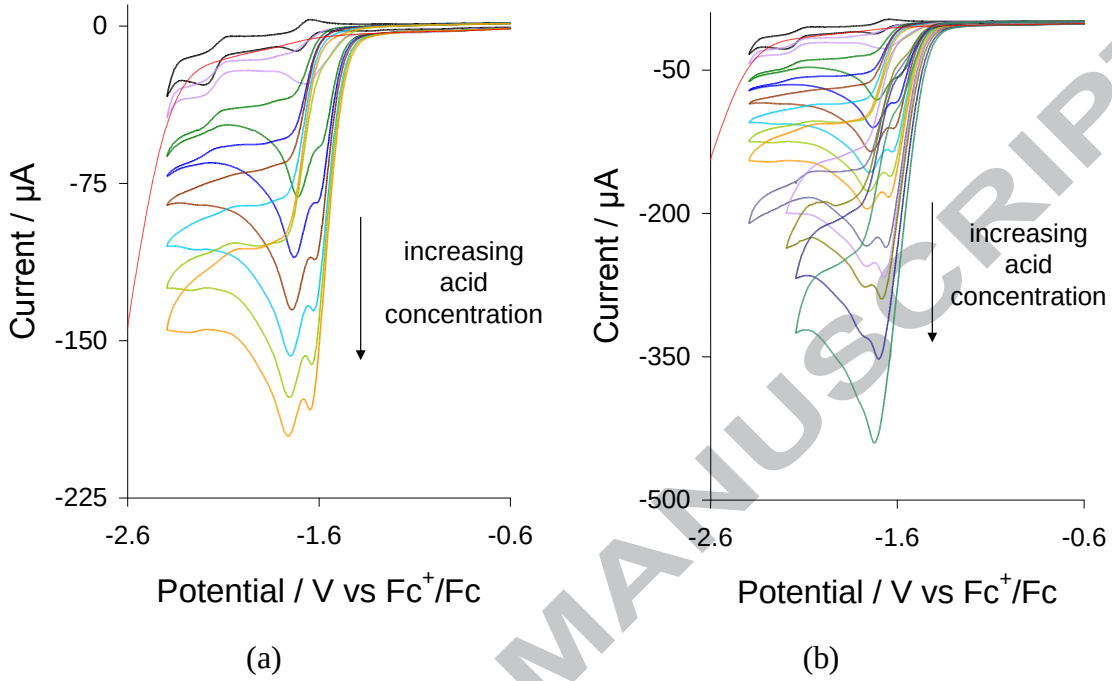

Fig. 6. CVs of **2** – (a) in the absence acid and in the presence of 1-7 equivalents of CF_3CO_2H, (b) in the absence acid and in the presence of 1-7, 9, 10, 12, 16 and 20 equivalents of CF_3CO_2H (in 1:1 CH_2Cl_2/MeCN, 1 mM solution, supporting electrolyte $[NBu_4][PF_6]$, scan rate 0.1 Vs^{-1}, glassy carbon electrode, potential vs Fc^+/Fc). Response of 20 equivalents CF_3CO_2H alone is shown with the red dashed line.

Fig. 7 shows a plot of catalytic current/noncatalytic current ratio (i_{cat}/i_p) *vs* acid concentration for the first catalytic wave. The i_{cat}/i_p value (used to measure the efficiency of a catalyst) increases to 33 after addition of 20 equivalents CF_3CO_2H, being similar to the most efficient cobalt and nickel mononuclear catalysts such as $(dmgBF_2)_2Co(NCMe)_2$ ($dmgBF^2$ = difluoroboryl-dimethylglyoxime) (i_{cat}/i_p ~30) [28], $[(P^{Ph}{}_2N^{Ph}{}_2)Co(MeCN)_3]^{2+}$ ($P^{Ph}{}_2N^{Ph}$ = 1,3,6-triphenyl-1-aza-3,6-diphosphacycloheptane) (i_{cat}/i_p ~30) [29] and $[(P^{Ph}{}_2N^{Ph})Ni]^{2+}$ (i_{cat}/i_p 38) [30].

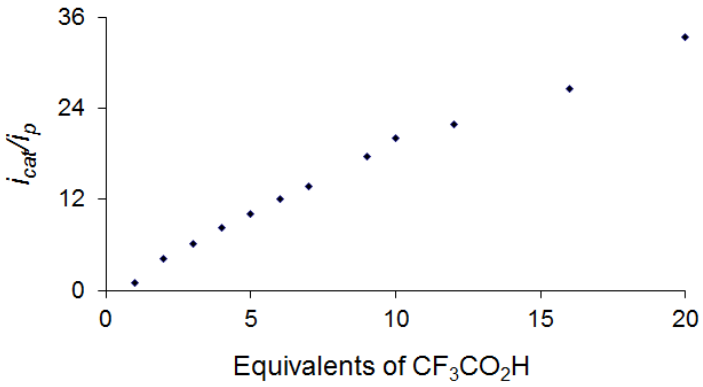

Fig. 7. Dependence of i_{cat}/i_p on CF_3CO_2H concentration for **2** at potentials of the first catalytic wave (in 1:1 CH_2Cl_2/MeCN, 1 mM solution, 1-20 equivalents $HBF_4{\cdot}Et_2O$, supporting electrolyte $[NBu_4][PF_6]$, scan rate 0.1 Vs^{-1}, glassy carbon electrode).

3. Conclusions

In summary, coordinatively and electronically unsaturated square-pyramidal Fe(CO)(κ^2-dppn)(κ^2-tbt) (**2**) has been synthesised and structurally characterised. It adopts a square-pyramidal geometry in the solid-state but is fluxional in solution being proposed to interconvert with a trigonal bipyramidal isomer. Cyclic voltammetry shows that it undergoes a reversible one-electron reduction, with DFT calculations showing that this is primarily ligand-based, the added electron being delocalised over the naphthalene backbone of the dppn ligand. This marks **2** out as being significantly different to related Fe(CO)(κ^2-diphosphine)(κ^2-dithiolate) complexes studied as proton-reduction catalysts, where the LUMO is primarily metal-centred and hence reduction affords an Fe(I) radical anion [6-8]. Nevertheless, **2** is found to be a highly efficient proton-reduction catalyst generating hydrogen from CF_3CO_2H at relatively mild potentials. Work is continuing to address the mechanism of proton-reduction, especially regarding the role of the redox-active dppn ligand [31], and hence to further develop this class of coordinatively and electronically unsaturated complexes as proton-reduction catalysts.

4. Experimental

4.1. General

Unless otherwise stated, all manipulations were carried out under a nitrogen atmosphere using standard Schlenk techniques. Reagent-grade solvents were dried using appropriate drying agents and distilled prior to use by standard methods. Infrared spectra were recorded on a Shimadzu FTIR 8101 spectrophotometer. NMR spectra were recorded on a Bruker DPX 400 instrument. Elemental analysis was performed by Microanalytical Laboratories, University College London. $Fe_2(CO)_6(\mu\text{-tdt})$ was prepared according to a published procedure [32].

4.2. Reaction of $Fe_2(CO)_6(\mu\text{-tdt})$ with dppn

An acetonitrile solution (15 mL) of $Fe_2(CO)_6(\mu\text{-tdt})$ (100 mg, 0.23 mmol), $Me_3NO{\cdot}2H_2O$ (18 mg, 0.23 mmol) and dppn (114 mg, 0.23 mmol) was heated to reflux for 1 h. The reaction mixture was then allowed to cool at room temperature. The solvent was removed by rotary evaporation under reduced pressure and the residue chromatographed by TLC on silica gel. Elution with hexane/CH_2Cl_2 (4:1, v/v) developed two bands. The red band gave $Fe_2(CO)_4(\kappa^2\text{-dppn})(\mu\text{-tdt})$ (**1**) (70 mg, 35 %) as deep red crystals, while the green band gave $Fe(CO)(\kappa^2\text{-dppn})(\kappa^2\text{-tdt})$ (**2**) (20 mg, 12%) as dark green crystals after recrystallization from hexane/CH_2Cl_2 at 4 °C. Data for **1**: Anal. calc. for $C_{45}H_{32}Fe_2O_4P_2S_2$ (found): C 61.80 (62.39), H 3.69 (3.76). IR (νCO)(CH_2Cl_2): 2021s, 1950m, 1907w cm^{-1}. ^1H NMR ($CDCl_3$): δ 8.12 (d, J 8.0, 2H), 7.92 (d, J 8.0, 1H), 7.88 (s, 1H), 7.48 (m, 13H), 6.89 (m, 3H), 6.66 (m, 9H), 2.34 (3H, s). $^{31}P\{^1H\}$ NMR ($CDCl_3$): δ 69.5 (s). Data for **2**: Anal. calc. for $C_{42}H_{32}FeOP_2S_2{\cdot}CHCl_3$ (found): C 60.48 (60.93), H 3.89 (3.97). IR (νCO)(CH_2Cl_2): 1918s cm^{-1}. ^1H NMR ($CDCl_3$): δ 8.16 (d, J 7.04 Hz, 2H), 7.96 (d, J 8.08 Hz, 2H), 7.91 (s, 1H), 7.58-7.51 (m, 14H), 6.95 (m, 3H), 6.69 (m, 7H), 2.37 (s, 3H). $^{31}P\{^1H\}$ NMR ($CDCl_3$): δ 67.9 (s).

4.3. Crystal structure determinations

Single crystals of **1** and **2** suitable for diffraction analysis were grown by slow diffusion of hexane into a dichloromethane solution at 4 °C. All geometric and crystallographic data for **1** were collected at 150 K on a Bruker SMART APEX CCD diffractometer using Mo-Kα radiation (λ = 0.71073). Data collection, indexing and initial cell refinements were all done using SMART [33] software. Data reduction were carried out with SAINT PLUS [34] and absorption corrections applied using the programme SADABS [35]. Structures were solved

by direct methods and developed using alternating cycles of least-squares refinement and difference-Fourier synthesis. All non-hydrogen atoms were refined anisotropically. Hydrogens were placed in calculated positions (riding model). Structure solution used SHELXTL PLUS V6.10 program package [36]. A suitable single crystal of **2** was mounted on an Agilent Super Nova dual diffractometer (Agilent Technologies Inc., Santa Clara, CA) using a Nylon Loop and the diffraction data were collected at 134(1) K using Cu-Kα radiation (λ = 1.54184). Unit cell determination, data reduction, and absorption corrections were carried out using CrysAlisPro [37]. The structures were solved with the ShelXS [36] structure solution program by direct methods and refined with the XL [36] refinement package using Least Squares minimisation within the OLEX2 [38] graphical user interface. Non-hydrogen atoms were refined anisotropically, and hydrogen atoms were included using a riding model. The details of the data collection and structure refinement are given in Table 1.

4.4. Density functional theory (DFT) calculations

All calculations were performed with the hybrid DFT functional B3LYP, as implemented by the Gaussian 09 program package [39]. This functional utilizes the Becke three-parameter exchange functional (B3) [40], combined with the correlation functional of Lee, Yang and Parr (LYP) [41]. The iron atom was described by Stuttgart–Dresden effective core potential (ecp) and SDD basis set, while the 6-31+G(d′) basis set was employed for the remaining atoms. All computed species were established as intermediates or minima based on zero imaginary frequencies (positive eigenvalues). The computed frequencies were used to make zero-point and thermal corrections to the electronic energies; the reported energies are quoted in kJ mol^{-1} relative to the specified standard. The natural charges and Wiberg bond indices reported here were computed using Weinhold's natural bond orbital (NBO) program [42,43]. The geometry-optimized structures have been drawn with the JIMP2 molecular visualization and manipulation program [44,45].

4.5. Electrochemical Studies

Electrochemistry was carried out either in deoxygenated CH_2Cl_2 or a 1:1 mixture of CH_2Cl_2/MeCN with 0.1 M $TBAPF_6$ as the supporting electrolyte. The working electrode was a 3 mm diameter glassy carbon electrode that was polished with 0.3 μm alumina slurry prior to each scan. The counter electrode was a Pt wire and the quasi-reference electrode was a

silver wire. All CVs were referenced to the Fc^+/Fc redox couple. An Autolab potentiostat (EcoChemie, Netherlands) was used for all electrochemical measurements. Catalysis studies were carried out by adding equivalents of CF_3CO_2H (Sigma-Aldrich).

Acknowledgements

We thank the Commonwealth Scholarship Commission for the award of a Commonwealth Scholarship to SG. MGR acknowledges financial support from the Robert A. Welch Foundation (Grant B-1093) and the NSF (CHE-0741936). Prof. Michael B. Hall (TAMU) is thanked for providing us a copy of his JIMP2 program, which was used to prepare the geometry optimized structures reported here. GH thanks King's College London for Funding.

Appendix A. Supplementary material

CCDC 1825298 (for **1**) and CCDC 1825299 (for **2**) contain the supplementary crystallographic data for this paper. These data can be obtained free of charge from The Cambridge Crystallographic Data Centre via www.ccdc.cam.ac.uk/data_request/cif.

Table 1 Crystallographic data for **1** and **2**

Compound	**1**	**2**
Empirical formula	$C_{45}H_{32}Fe_2O_4P_2S_2$	$C_{42}H_{32}FeOP_2S_2{\cdot}CHCl_3$
Formula weight	874.47	853.95
Temp (K)	150 (2)	134(1)
Wavelength (Å)	0.71073	1.54184
Crystal system	Triclinic	Monoclinic
Space group	*P*-1	$P2_1/c$
a (Å)	10.6010(9)	15.78692(17)
b (Å)	13.1222(11)	13.69980(17)
c (Å)	15.4847(13)	18.0806(2)
α (°)	91.417(2)	90
β (°)	106.046(1)	102.5994(11)
γ (°)	108.993(1)	90
Volume ($Å^3$)	1941.8(3)	3816.27(8)
Z	2	4
Calculated density (gcm^{-3})	1.496	1.486
Absorption coefficient (mm^{-1})	0.982	7.191
F(000)	896	1752
Crystal size (mm^3)	0.10 × 0.09 × 0.04	0.27 × 0.11 × 0.05
2θ range for data collection (°)	5.52 to 56.52	8.17 to 134.984
Index ranges	$-14 \le h \le 14$	$-18 \le h \le 18$
	$-17 \le k \le 17$	$-16 \le k \le 10$
	$-20 \le l \le 20$	$-19 \le l \le 21$
Reflections collected	17013	12220
Independent reflections (R_{int})	8946 (R_{int} = 0.0303)	6718 (R_{int} = 0.0364)
Data/restraints/parameters	8946 / 0 / 496	6718 / 0 / 470
Goodness-of-fit on F^2	1.068	1.036
Final *R* indices [$I > 2\sigma(I)$]	R_1 = 0.0471,	R_1 = 0.0426,
	wR_2 = 0.0988	wR_2 = 0.1036
R indices (all data)	R_1 = 0.04603,	R_1 = 0.0517,
	wR_2 = 0.1041	wR_2 = 0.1116
Largest difference in peak and hole (e $Å^{-3}$)	0.548 and –0.361	0.70 and –0.53

References

1 I. Bhugun, D. Lexa and J.-M. Saveánt, *J. Am. Chem. Soc.,* 1996, **118**, 3982-3983.

2 M.J. Rose, H.B. Gray and J.R. Winkler, *J. Am. Chem. Soc.,* 2012, **134**, 8310-8313.

3 V. Artero and M. Fontecave, *C. R. Chimie,* 2008, **11**, 926-931.

4 G.P. Connor, K.J. Mayer, C.S. Tribble and W.R. McNamara, *Inorg. Chem.*, 53 (2014) 5408-5410.

5 S. Kaur-Ghumaan, L. Schwartz, R. Lomoth, M. Stein and S. Ott, *Angew. Chem. Int. Ed.,* 2010, **49**, 8033-8036.

6 M. Beyler, S. Ezzaher, M. Karnahl, M.-P. Santoni, R. Lomoth and S. Ott, *Chem. Commun.,* 2011, **47**, 11662-11664.

7 A. Orthaber, M. Karnahl, S. Tschierlei, D. Streich, M. Stein and S. Ott, *Dalton Trans.,* 2014, **43**, 4537-4549.

8 S. Roy, S.K.S. Mazinani, T.L. Groy, L. Gan, P. Tarakeshwar, V. Mujica and A.K. Jones, *Inorg. Chem*., 2014, **53**, 8919-8929.

9 L. Gan, T.L. Groy, P. Tarakeshwar, S.K.S. Mazinani, J. Shearer, V. Mujica and A.K. Jones, *J. Am. Chem. Soc.,* 2015, **137**, 1109-1115.

10 G.-G. Luo, Y.-H. Wang, J.-H. Wang, J.-H. Wu and R.-B. Wu, *Chem. Commun.,* 2017, **53**, 7007-7010.

11 S. Gao, J. Fan, S. Sun, F. Song, X. Peng, Q. Duan, D. Jiang and Q. Liang, *Dalton Trans.,* 2012, **41**, 12064-12074.

12 A. Rana, B. Mondal, P. Sen, S. Dey and A. Dey**,** *Inorg. Chem.*, 2017, **56**, 1783-1793.

13 S. Ghosh, N. Hollingsworth, M. Warren, K.B. Holt and G. Hogarth, *Polyhedron,* 2017, **137**, 140-146.

14 V.W.-W. Yam and S.W.-K. Choi, *J. Chem. Soc., Dalton Trans.,* 1996, 4227-4232.

15 S.L. James, A.G. Orpen and P.G. Pringle, *J. Organomet. Chem.*, 1996, **525**, 299-301.

16 V.W.-W. Yam, C.-L. Chan, S.W.-K. Choi, K.M.-C. Wong, E.C.-C. Cheng, S.-C. Yu, P.-K. Ng, W.-K. Chan and K.-K. Cheung, *Chem. Commun.*, 2000, **1**, 53-54.

17 V.W.-W. Yam, C.-K. Li, C.-L. Chan and K.-K. Cheung, *Inorg. Chem.,* 2001, **40**, 7054-7058.

18 M.I. Bruce, P.A. Humphrey, S. Okucu, R. Schmutzler, B.W. Skelton and A.H. White, *Inorg. Chim. Acta*, 2004, **357**, 1805-1812.

19 M.I. Bruce, P.A. Humphrey, R. Schmutzler, B.W. Skelton and A.H. White, *J. Organomet. Chem.*, 2004, **689**, 2415-2420.

20 W.H. Watson, S. Kandala and M.G. Richmond, *J. Organomet. Chem.*, 2007, **692**, 968-975.

21 V.N. Nesterov, W.H. Watson, S. Kandala and M.G. Richmond, *Polyhedron*, 2007, **26**, 3602-3608.

22 S.E. Kabir, F. Ahmed, S. Ghosh, M.R. Hassan, M.S. Islam, A. Sharmin, D.A. Tocher, D.T. Haworth, S.V. Lindeman and T.A. Siddiquee, *J. Organomet. Chem.*, 2008, **693**, 2657-2665.

23 S. Ghosh, G. Hogarth, S.E. Kabir, A.L. Miah, L. Salassa, S. Sharmin and C. Garino, *Organometallics*, 2009, **28**, 7047-7052.

24 A. Rahaman, F.R. Alam, S. Ghosh, D.A. Tocher, M. Haukka, S.E. Kabir, E. Nordlander and G. Hogarth, *J. Organomet. Chem.*, 2014, **751**, 326-335.

25 A. Rahaman, S. Ghosh, D.G. Unwin, S. Basak-Modi, K.B. Holt, S.E. Kabir, E. Nordlander, M.G. Richmond and G. Hogarth, *Organometallics*, 2014, **33**, 1356-1366.

26 J.M. Camara and T.B. Rauchfuss, *J. Am. Chem. Soc.*, 2011, **133**, 8098-8101.

27 M.M. Hassan, M.B. Hursthouse, S.E. Kabir and K.M.A. Malik, *Polyhedron*, 2001, **20**, 97-101.

28 X. Hu, B. S. Brunschwig and J. C. Peters, *J. Am. Chem. Soc.*, 2007, **129**, 8988-8998.

29 G.M. Jacobsen, J.Y. Yang, B. Twamley, A.D. Wilson, R.M. Bullock, M. Rakowski-DuBois and D.L. DuBois, *Energy Environ. Sci.*, 2008, **1**, 167-174.

30 M.L. Helm, M.P. Stewart, R.M. Bullock, M. Rakowski-DuBois and D.L. DuBois, *Science*, 2011, **333**, 863-866.

31. S. Ghosh, S. Rana, N. Hollingsworth, M.G. Richmond, S.E. Kabir and G. Hogarth, *Inorganics*, submitted.

32 R.B. King, *J. Am. Chem. Soc.*, 1963, **85**, 1584-1587.

33 SMART Version 5.628; Bruker AXS, Inc., 5465 East Cheryl Parkway, Madison, WI 53711-5373, 2003.

34 SAINT Version 6.36A; Bruker AXS, Inc., 5465 East Cheryl Parkway, Madison, WI 53711-5373, 2002.

35 G.M. Sheldrick, SADABS Version 2.10; University of Göttingen, Göttingen, Germany, 2003.

36 G.M. Sheldrick, *Acta Crystallogr.*, 2008, **A64**,112-122.

37 CrysAlisPro; Oxford Diffraction: Yarnton, England, 2015.

38 O.V. Dolomanov, L.J. Bourhis, R.J. Gildea, J.A.K. Howard and H. Puschmann, *J. Appl. Cryst.*, 2009, **42**, 339-341.

39 M.J. Frisch, G.W. Trucks, H.B. Schlegel, G.E. Scuseria, M.A. Robb, J.R. Cheeseman, G. Scalmani, V. Barone, B. Mennucci, G.A. Petersson, H. Nakatsuji, M. Caricato, X. Li, H.P. Hratchian, A.F. Izmaylov, J. Bloino, G. Zheng, J.L. Sonnenberg, M. Hada, M. Ehara, K. Toyota, R. Fukuda, J. Hasegawa, M. Ishida, T. Nakajima, Y. Honda, O. Kitao, H. Nakai, T. Vreven, J. A. Montgomery Jr., J.E. Peralta, F. Ogliaro, M. Bearpark, J.J. Heyd, E. Brothers, K.N. Kudin, V.N. Staroverov, R. Kobayashi, J. Normand, K. Raghavachari, A. Rendell, J.C. Burant, S.S. Iyengar, J. Tomasi, M. Cossi, N. Rega, J.M. Millam, M. Klene, J.E. Knox, J.B. Cross, V. Bakken, C. Adamo, J. Jaramillo, R. Gomperts, R.E. Stratmann, O. Yazyev, A.J. Austin, R. Cammi, C. Pomelli, J.W. Ochterski, R.L. Martin, K. Morokuma, V.G. Zakrzewski, G.A. Voth, P. Salvador, J.J. Dannenberg, S. Dapprich, A.D. Daniels, O. Farkas, J.B. Foresman, J.V. Ortiz, J. Cioslowski and D.J. Fox, GAUSSIAN 09 (Revision A.02), Gaussian, Inc., Wallingford, CT, 2009.

40 A.D. Becke, *J. Chem. Phys.*, 1993, **98**, 5648-5652.

41 C. Lee, W. Yang and R.G. Parr, *Phys. Rev. B: Condens. Matter*, 1988, **37**, 785-789.

42 A.E. Reed, L.A. Curtiss and F. Weinhold, *Chem. Rev.*, 1988, **88**, 899-926.

43 K.B. Wiberg, *Tetrahedron*, 1968, **24**, 1083-1096.

44 JIMP2, version 0.091, a free program for the visualization and manipulation of molecules: M.B. Hall and R.F. Fenske, *Inorg. Chem.*, 1972, **11**, 768-775.

45 J. Manson, C.E. Webster and M.B. Hall, Texas A&M University, College Station, TX, 2006, http://www.chem.tamu.edu/jimp2/index.html.

Graphic abstract

Coordinatively and electronically unsaturated square-pyramidal Fe(CO)(κ^2-dppn)(κ^2-tdt) is shown to be amongst the most efficient proton-reduction catalysts reported to date. Catalysis occurs at the first reduction potential and it displays an impressive i_{cat}/i_p ratio of 33 after addition of 20 equivalents CF_3CO_2H.

Graphic

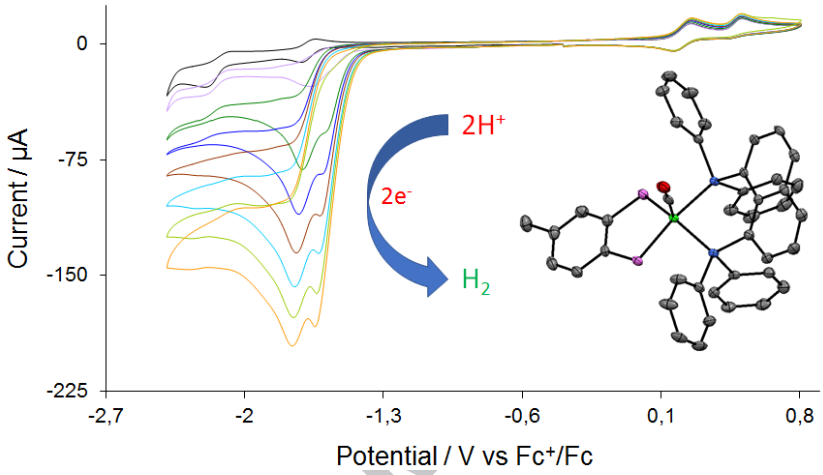

Highlights

- Synthesis of coordinatively and electronically unsaturated Fe(CO)(κ^2-dppn)(κ^2-tdt)
- CV and DFT studies reveal nature of mono-anion
- Efficient proton-reduction catalyst at first reduction potential